ISSN 1990-7931, Russian Journal of Physical Chemistry B, 2022, Vol. 16, No. 5, pp. 1008–1014. © Pleiades Publishing, Ltd., 2022.
Russian Text © The Author(s), 2022, published in Khimicheskaya Fizika, 2022, Vol. 41, No. 10, pp. 84–90.

CHEMICAL PHYSICS OF ATMOSPHERIC PHENOMENA

Prerequisites for the Modification of the Block for Calculating the Electric Potential in the Ionosphere in the Model of the Upper Atmosphere

V. V. Klimenko[a], V. V. Denisenko[b], and M. V. Klimenko[a, *]

[a] *Pushkov Institute of Terrestrial Magnetism, Ionosphere and Radio Wave Propagation, Kaliningrad Branch, Russian Academy of Sciences, Kaliningrad, Russia*

[b] *Institute of Solar-Terrestrial Physics, Siberian Branch, Russian Academy of Sciences, Irkutsk, Russia*

**e-mail: maksim.klimenko@mail.ru*

Received April 19, 2022; revised May 6, 2022; accepted May 20, 2022

Abstract—The results of comparing the accuracy and speed of two numerical algorithms for calculating the electric potential in the Earth's ionosphere are presented. Several test problems for which exact analytical solutions are available are considered. It is shown that both approaches can be used to calculate the electric potential in models of the upper atmosphere, including in the regions of the equatorial electric jet. The combined use of the finite element method and the Fedorenko multigrid method with a preliminary transition to the problem for special potentials leads to a much more accurate and faster solution of the two-dimensional electrical conductivity equation in the ionosphere than the method used earlier in the block for calculating the electric potential of the global self-consistent model of the thermosphere–ionosphere–protonosphere.

Keywords: ionosphere, electric field, numerical simulation

DOI: 10.1134/S1990793122050219

1. INTRODUCTION

The ionosphere is the propagation medium for radio waves. Terrestrial radio communications, navigation of aircraft and ships, radar, and direction finding are carried out through it. Therefore, it is necessary to foresee those (sometimes catastrophic) changes in the parameters of the ionosphere which lead to disruption and sometimes to the complete disappearance of radio communication [1]. Electric fields and currents have a significant effect on the heat balance, dynamics, and structure of the upper atmosphere at all latitudes [2–5]. Their role especially increases during periods of magnetospheric disturbances, when the ionosphere experiences significant changes [6–9].

In order to obtain a spatiotemporal picture of the variations of the electric field in the ionosphere, there are not enough observational data either under calm conditions or, even more so, during geomagnetic storms in each specific case. Self-consistent models of the Earth's upper atmosphere are currently helping us to eliminate this shortcoming [10, 11]. One of the main mechanisms of plasma transport in the Earth's ionosphere is electromagnetic drift, which is important to correctly take into account when modeling the ionosphere, especially the upper one. To study the space-time distribution of the electric field in the Earth's ionosphere and the physical mechanisms of its generation, numerical models of the electric field in the ionosphere are being developed. Due to the existence of two main types of electric fields in the ionosphere (of ionospheric and magnetospheric origin), there are two types of numerical models: the electric dynamo field in the Earth's ionosphere [12–15] and the electric field of magnetospheric convection [3, 16–19]. Note that sometimes a third source should be taken into account, namely, the global electric circuit associated with lightning activity [20] and the fields of underground generators [21], the electric field of which is taken into account only in individual cases, although at night it can be important.

In the existing global numerical models, the potential of a large-scale electric field is found from the solution of the two-dimensional electrical conductivity equation, which is obtained from the three-dimensional balance equation of the total current in the ionosphere by integrating it along the geomagnetic field lines under the assumption that the longitudinal conductivity is infinite. For example, a block for calculating the potential of the electric field in the global self-consistent model of the thermosphere–ionosphere–protonosphere (GSM TIP) is organized [22–24]. The results of calculations by this model were used to interpret variations in ionospheric parameters under quiet geomagnetic conditions and during geomagnetic

storms [25–27]. It should be noted that, in the block for calculating the electric field of the GSM TIP model, a method for solving an elliptic two-dimensional equation for the electric potential in the ionosphere is used, which has an insufficiently high accuracy and convergence rate. Preliminary estimates have shown that, as a result, the time costs increase significantly when carrying out numerical calculations using the GSM TIP model. In this article, we present the results of comparing the accuracy and speed of two numerical algorithms for calculating the electric potential in the Earth's ionosphere.

2. STATEMENT OF THE PROBLEM OF MODELING THE ELECTRIC FIELD

The basic equations for stationary electric field **E** and current density **j** in the Earth's ionosphere that we use in our numerical models are the equations describing Faraday's law, the law of conservation of charge, and Ohm's law:

$$\mathrm{rot}\mathbf{E} = 0, \quad (1)$$

$$\mathrm{div}\mathbf{j} = q, \quad (2)$$

$$\mathbf{j} = \hat{\sigma}\mathbf{E}, \quad (3)$$

where $\hat{\sigma}$ is the conductivity tensor; **q** is the local time derivative of the electric charge density brought by the external current, which in a stationary process must be compensated by the conduction current [28]. Because vector function **E** satisfies Eq. (1), electric potential V, can be introduced such that

$$\mathbf{E} = -\mathrm{grad}V. \quad (4)$$

Then system of equations (1)–(3) is reduced to the electrical conductivity equation:

$$-\mathrm{div}\left(\hat{\sigma}\mathrm{grad}V\right) = q. \quad (5)$$

Three-dimensional equation (5) is reduced to a two-dimensional form by integrating over the thickness of the current-conducting layer of the ionosphere along the geomagnetic field lines, the conductivity along which is much greater than the transverse conductivities. We solve this two-dimensional equation using two models. In the first model (hereinafter referred to as model 1 [23]) used in the GSM TIP model, the solution of the elliptic equation (5), written in the difference form, is carried out by the method of successive lower relaxation with a relaxation parameter equal to 0.9. The iterative process is carried out with a predetermined accuracy of 10^{-6}. This model of the electric field was used to study the effect of atmospheric tides [29] and magnetospheric–ionospheric current systems [24] on the distribution of the electric potential in the ionosphere.

Another model (hereinafter referred to as model 2) is presented in [30, 31]. The article [32] describes how to replace the boundary value problem for the electric potential in the ionosphere with a problem with a self-adjoint positive definite operator for special potentials, and the principle of the minimum of the quadratic energy functional is proved. This allows minimizing the functional instead of solving the boundary value problem. This variational principle is useful for obtaining an approximate or numerical solution, since it allows the use of many classical algorithms. The numerical method for such a problem is described in detail in the book [33], including a new statement of the boundary value problem, the finite element method, the multigrid method, and some test calculations. The finite element method uses regular inhomogeneous grids and piecewise linear approximating functions. The equations of the finite element method are obtained as conditions for the minimum of the energy functional. Fedorenko's multigrid method is used to solve this system of linear algebraic equations. The effectiveness of the developed multigrid method has been shown in testing and calculating electric fields and currents in the Earth's ionosphere, including the model presented in [34]. Typical examples are discussed below.

3. DESCRIPTION OF TEST BOUNDARY VALUE PROBLEMS

To compare the numerical results of the two models described above with analytical solutions, we considered several idealized cases. When modeling the electric field in the Earth's ionosphere, spherical geomagnetic coordinates are most often used: colatitude and longitude, θ_m, φ_m; the geomagnetic latitude $\lambda_m = (\pi/2) - \theta_m$. Let us build some reference area on the plane with Cartesian coordinates x, y, the points of which identify all the magnetic field lines of interest to us [30]. Let us transform the Northern Hemisphere into a unit circle with polar coordinates (radius $\rho < 1$ and angle $0 < \alpha < 2\pi$):

$$\rho = 1.5\sin(\theta_m)\Big/\left[1 + \left(1 - 0.75\sin^2(\theta_m)\right)^{1/2}\right], \quad \alpha = \varphi_m.$$

We conformally transform the resulting circle into a strip $0 < x < 2\pi$, $y > 0$:

$$y = -\ln(\rho), \quad x = \alpha.$$

Because $x = \alpha = \varphi_m$, we are interested in a solution that is periodic in x. The constructed band has no physical meaning, but it is convenient for a numerical solution and helps avoid the difficulties associated with the peculiarity of conductivity in the equatorial ionosphere [35]. In such a strip, after the necessary geometric transformation, the two-dimensional electrical conductivity equation obtained from Eq. (5) looks like this:

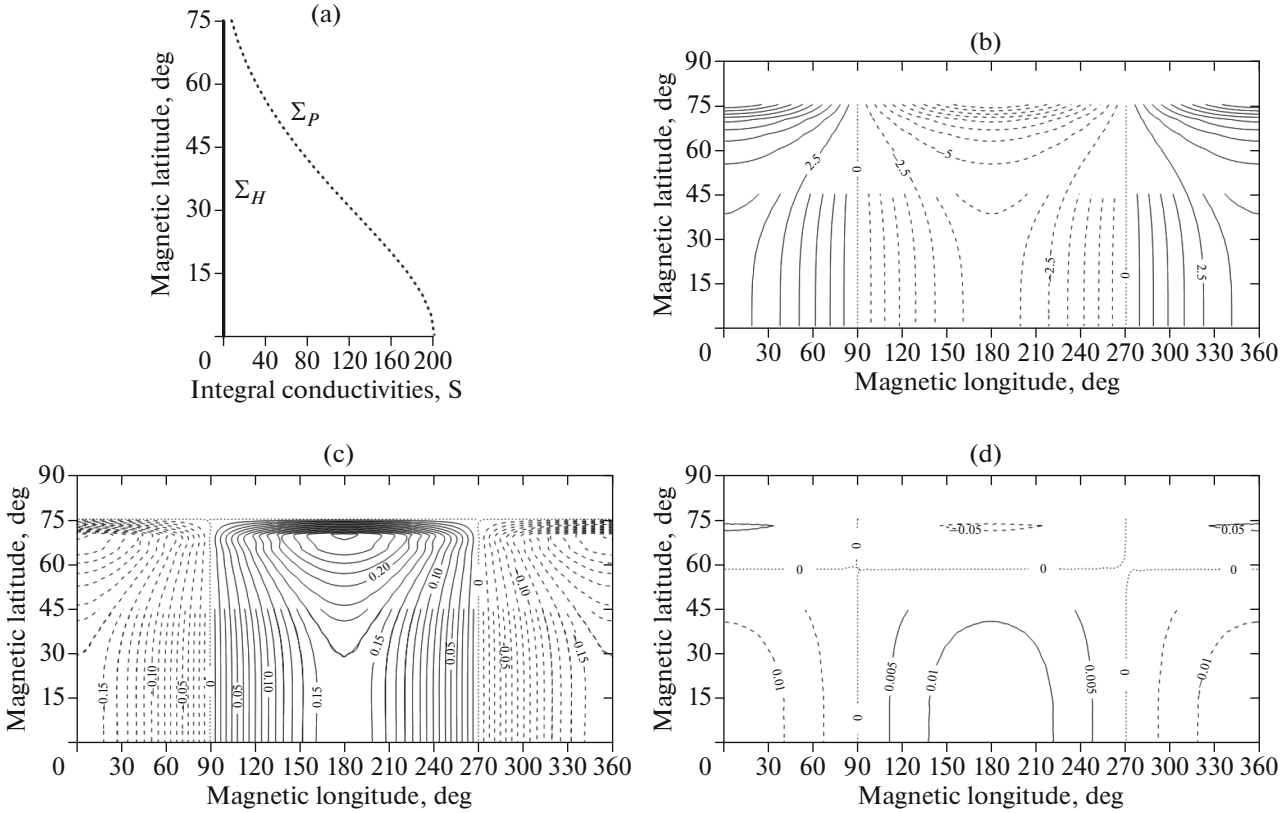

Fig. 1. Input parameters and calculation results for the third task: (a) latitudinal profiles of the Hall (solid line) and Pedersen (dotted line) conductivities; (b) isolines of the analytical solution for the electric potential in kV; and (c, d) isolines of errors in calculating the potential in kV in models 1 and 2, respectively, in the form of differences between the analytical and numerical solutions.

$$-\frac{\partial}{\partial x}\left(\Sigma_P\frac{\partial V}{\partial x}+\Sigma_H\frac{\partial V}{\partial y}\right)$$
$$-\frac{\partial}{\partial y}\left(-\Sigma_H\frac{\partial V}{\partial x}+\Sigma_P\frac{\partial V}{\partial y}\right)=Q, \quad (6)$$

where Σ_P and Σ_H are the Pedersen and Hall integral conductivities [28] and Q generally defined by three sources. First, this is the divergence of the external current inside the ionosphere, i.e., the right side of Eq. (2) integrated along the magnetic field line. Secondly, it is atmospheric currents J^N_{atm} and J^S_{atm}, entering the ionosphere through the ends of the magnetic field line in the Northern and Southern hemispheres. Thirdly, it is magnetospheric–ionospheric field-aligned currents. In the test problems under consideration, atmospheric and magnetospheric–ionospheric currents are absent.

The border $y = 0$ corresponds to the lowest magnetic field lines, which are considered ionospheric. Their peaks are on high $h_{eq} = 90$ km at the geomagnetic equator, while their lowest points are at $h_1 = 80$ km. This avoids the zero length of these last lines and the associated zero coefficients in Eq. (6). It also makes the right hand side in the boundary condition derived from the charge conservation law nonzero:

$$\left(-\Sigma_H\frac{\partial V}{\partial x}+\Sigma_P\frac{\partial V}{\partial y}\right)\Big|_{y=0}=J^0_{eq}(x), \quad (7)$$

where $J^0_{eq}(x)$ includes atmospheric currents J^N_{atm} and J^S_{atm}, entering the ionosphere through the lowest magnetic field lines. The consideration of conductors in the magnetosphere [31] shows that auroral zones are equivalent to almost ideal conductors, since they are connected parallel with good magnetospheric conductors. We approximate them as ideal conductors with a given electric potential distribution V. Therefore, the boundary condition has the form

$$V|_{y=y_{aur}(x)}=V_{aur}(x). \quad (8)$$

The partial differential equation (6) is an elliptic type equation, and the boundary value problem (6)–(8) has a unique solution [32].

The integral conductivities calculated on the noon meridian at low solar activity on the day of the vernal equinox are approximated using the following formulas:

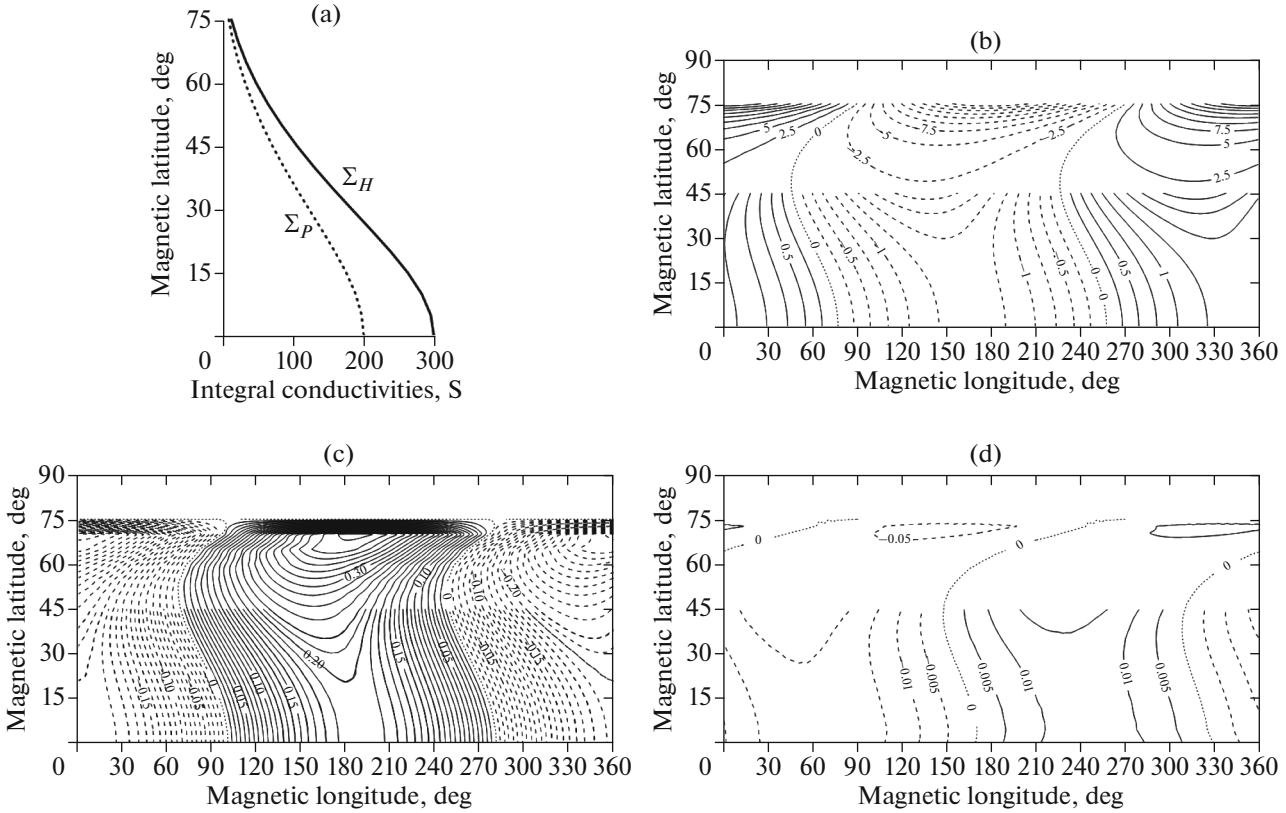

Fig. 2. Same as in Fig. 1 for the fourth task.

$$\Sigma_P = \Sigma_0 \exp\{-\mu(y - y_e)\}, \quad \Sigma_H = \beta\Sigma_P, \quad y_e < y < y_a,$$
$$\Sigma_P = \Sigma_e, \quad \Sigma_H = \beta_e\Sigma_e, \quad 0 < y < y_e, \tag{9}$$

where $\Sigma_0, \mu, \beta, \beta_e, \Sigma_e$ are given constants. To simplify the calculations, we assume the continuity of the Hall conductivity: $\beta\Sigma_0 = \beta_e\Sigma_e$. The layer corresponding to $y < y_e$ is a narrow strip near the border $y = 0$ and corresponds to the region of equatorial electric jets. We presume $y_e = 0.00615$ and $y_a = 1.6265$, which corresponds to the height $h = 120$ km and latitude 75° and set the following values: $\Sigma_0 = 200$ S, $\beta = 1.5$, $\mu = 2$, $\Sigma_e = 10$ S, and $\beta_e = 30$. The latter give the Cowling conductivity value $\Sigma_C = 9010$ S, whose integral in the region of the electric jet $90 < h < 120$ km is about 270 MS m, like in the real midday ionosphere. Boundary conditions (7) and (8) in the test have the form

$$J_y\big|_{y=0} = 0, \quad V\big|_{y=y_a} = V_0 \cos x, \tag{10}$$

where $V_0 = 25$ kV.

We find the exact solution of problem (6), (10) as the real part of the complex function $V(x, y)$.

At $0 < y < y_e$,

$$V(x, y) = \xi[V_3 \exp(y - y_e) + V_4 \exp(y_e - y)]e^{ix},$$

where

$$V_3 = \left[1 + \frac{1 - i\beta_e}{1 + i\beta_e}\exp(-2y_e)\right]^{-1}, \quad V_4 = 1 - V_3,$$

where i is an imaginary unit.

At $y_e < y < y_a$,

$$V(x, y) = \xi(V_1 \exp\{\lambda_1(y - y_e)\} + V_2 \exp\{\lambda_2(y - y_e)\})e^{ix}, \tag{11}$$

where

$$\lambda_{1,2} = -\frac{\mu}{2} + \left[\left(\frac{\mu}{2}\right)^2 + 1 + i\beta\mu\right]^{1/2},$$
$$V_1 = \frac{1}{\lambda_1 - \lambda_2}\left[\frac{\Sigma_{P0}}{\Sigma_0}(V_3 - V_4) - \lambda_2\right], \quad V_2 = 1 - V_1,$$
$$\xi = V_0/[V_1 \exp\{\lambda_1(y_a - y_e)\} + V_2 \exp\{\lambda_2(y_a - y_e)\}].$$

If we exclude the region of the electric jet and determine in the entire region

$$\Sigma_P = \Sigma_0 \exp(-\mu y), \quad \Sigma_H = \beta\Sigma_P, \quad 0 < y < y_a,$$

we obtain a simpler test. For the same boundary conditions (see (10)), the exact solution has the form (11) with the same $\lambda_{1,2}$, but

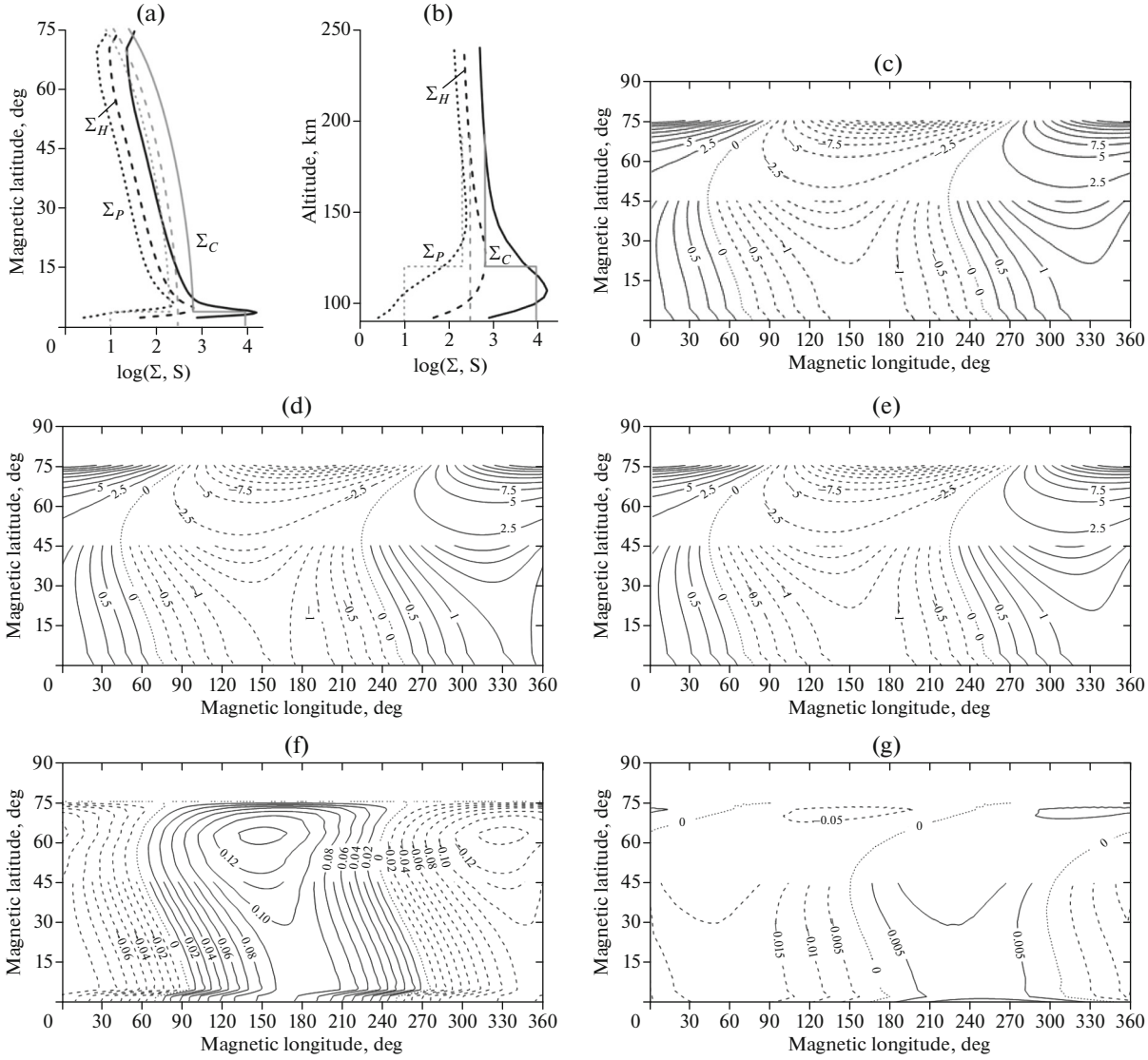

Fig. 3. Input parameters and calculation results for the fifth task: (a) latitudinal profiles of the Hall (dashed lines), Pedersen (dotted lines), and Cowling (solid lines) conductivities; (b) fragment of height profiles of these conductivities at the geomagnetic equator (black shows the conductivities calculated using the IRI model and gray shows the approximations of these conductivities described in Section 2); (c) isolines of the analytical solution for the electric potential in kV; (d, e) isolines of electric potential distributions in kV; (f, g) isolines of potential calculation errors in kV in models 1 and 2, respectively.

$$V_1 = \frac{-\lambda_2 + i\beta}{\lambda_1 - \lambda_2}, \quad V_2 = 1 - V_1,$$
$$\xi = V_0 / \left[V_1 \exp(\lambda_1 y_a) + V_2 \exp(\lambda_2 y_a)\right].$$

It is easy to ensure that this solution is obtained from the previous one for $y_e \to 0$.

4. RESULTS

To test the two methods we have chosen for solving the electrical conductivity equation for the electric potential in the Earth's ionosphere for accuracy and speed, five problems with exact analytical solutions were considered. The solution of the two simplest problems—in the first of which formulas (9) use the values $\Sigma_0 = 1$ S, $\mu = 0$, $\beta = 0$ at $0 < y < y_a$ (i.e., $\Sigma_P = 1$ S, and $\Sigma_H = 0$ cm) and in the second $\Sigma_0 = 1$ S, $\mu = 0$, $\beta = 1.5$ at $0 < y < y_a$ (i.e., $\Sigma_P = 1$ S, and $\Sigma_H = 1.5$ S)—is not given in this article. We only note the high accuracy of both methods in solving these two idealized problems. At the same time, the accuracy in the method used in model 2 is 4–6 times higher near the equator, and the computation time is 3 times less than in the method used in model 1.

In the third problem, formulas (9) considered the region $0 < y < y_a$ at $\Sigma_0 = 200$ S, $\mu = 2$, $\beta = 0$ (i.e., $\Sigma_P = 200\exp(-2y)$, and $\Sigma_H = 0$). For the case of the

3rd problem, Fig. 1 shows the latitudinal profiles of the Hall and Pedersen conductivities and the analytical solution in the absence of the Hall conductivity and with the Pedersen conductivity varying exponentially from the equator to high latitudes and constant in longitude. The same figure shows the errors of models 2 and 1 in the form of differences between the analytical and model solutions. It can be seen that the accuracy of model 2 is 5–15 times higher than that of model 1. The maximum error of model 1 was 0.15 kV near the equator and 0.3 kV at high latitudes, while the error of model 2 in the same place was 0.01 and 0.05 kV, respectively. At the same time, the counting time is 3–5 times less for model 2 compared to model 1.

In the fourth problem, just as in the three previous ones, in formulas (9) the area $0 < y < y_a$ at $\Sigma_0 = 200$ S, $\mu = 2$, $\beta = 1.5$ (i.e., $\Sigma_P = 200\exp(-2y)$, and $\Sigma_H = 300\exp(-2y)$). For the fourth problem, Fig. 2 shows the latitudinal profiles of the Hall and Pedersen conductivities and the analytical solution for the Pedersen and Hall conductivities varying exponentially from the equator to high latitudes and constant in longitude. This figure also shows the errors of models 2 and 1. It can be seen that the accuracy of model 2 is 8–20 times higher than that of model 1. The maximum error of model 1 was 0.2 kV near the equator and 0.4 kV at high latitudes, while the error of model 2 in the same place was 0.01 and 0.05 kV, respectively. At the same time, the counting time is 3 times less for model 2 compared to model 1.

The fifth, most general, problem is described in detail in Section 2. It differs from the previous ones in that it takes into account the region of the equatorial electrojet with high values of the Cowling conductivity Σ_C. For the fifth problem, Fig. 3 shows the latitudinal profiles of the Hall, Pedersen, and Cowling conductivities, a fragment of their altitude profiles at the geomagnetic equator, and functions approximating them, which make it possible to obtain an analytical solution. It should be noted that the given height profiles of conductivities are close to the mean climatic profiles obtained using the IRI reference model of the ionosphere [36] and presented in Figs. 3. The same figure shows the distributions of the electric potential and the errors obtained for this case in models 2 and 1. The differences between the analytical and model distributions of the electric potential for this case at high and middle latitudes are practically not visible. These differences increase near the equator. The accuracy of model 2 is 3–5 times higher than that of model 1. The maximum error of model 1 near the equator was 0.1 kV (~8%) and, at high latitudes, 0.15 kV (~0.6%), while the error of model 2 there was 0.015 kV (~1.5%) and 0.05 kV (~0.2%), respectively. In this case, the counting time is 3 times less for model 2.

Since the layer of equatorial electric jets corresponding to $0 < y < y_e$, corresponding to magnetic field lines whose peaks are in the height interval of 90–120 km (thousands of times thinner than the boundary length (40000 km)), it can be effectively studied as a boundary layer. Such a theory was developed by Richmond [37]. The corresponding modeling of the boundary layer with a special boundary condition replacing condition (7) was presented in the book [33], including the formulation of the problem with a self-adjoint positive definite operator and its numerical version. When using this modification of our numerical method, the computation time for the analyzed test is reduced by about 7 times, while the error remains the same.

5. CONCLUSIONS

This article presents the results of test calculations of two numerical models of the electric field potential in the Earth's ionosphere. The errors of the models obtained in solving various problems showed that both models can be used to calculate the electric potential in models of the upper atmosphere, including in the region of the equatorial electric jet. However, the combined use of the finite element method and the Fedorenko multigrid method with a preliminary transition to the problem for special potentials leads to a much more accurate and faster solution of the two-dimensional electrical conductivity equation in the ionosphere than the finite difference method used in the electric potential calculation unit of the GSM TIP model.

FUNDING

This work was financially supported by the Russian Science Foundation, grant no. 21-17-00208.

REFERENCES

1. D. S. Kotova, I. E. Zakharenkova, M. V. Klimenko, V. B. Ovodenko, I. V. Tyutin, D. V. Chugunin, A. A. Chernyshov, K. G. Ratovsky, N. V. Chirik, M. V. Uspensky, V. V. Klimenko, R. A. Rakhmatulin, A. Yu. Pashin, A. V. Dmitriev, and A. V. Suvorova, Russ. J. Phys. Chem. B **14**, 377 (2020).
2. M. I. Pudovkin, Space Sci. Rev. **16**, 727 (1974).
3. V. V. Denisenko, N. V. Erkaev, A. V. Kitaev, and I. T. Matveenkov, *Mathematical Modeling of Magnetospheric Processes* (Nauka, Novosibirsk, 1992) [in Russian].
4. R. A. Heelis, J. Atmos. Sol.-Terr. Phys. **66**, 825 (2004).
5. M. A. Abdu, Adv. Space Res. **35**, 771 (2005).
6. V. B. Lyatskii, *Current Systems of Magnetospheric-Ionospheric Disturbances* (Nauka, Leningrad, 1978) [in Russian].
7. E. A. Ponomarev, *Mechanisms of Magnetospheric Substorms,* Ed. by Yu. I. Gal'perin (Nauka, Moscow, 1985) [in Russian].
8. R. A. Wolf, R. W. Spiro, S. Sazykin, and F. R. Toffoletto, J. Atmos. Sol.-Terr. Phys. **69**, 288 (2007).

9. M. G. Golubkov, A. V. Suvorova, A. V. Dmitriev, and G. V. Golubkov, Russ. J. Phys. Chem. B **14**, 873 (2020).
10. N. Maruyama, A. D. Richmond, T. J. Fuller-Rowell, et al., Geophys. Rev. Lett. **32**, L17105 (2005).
11. M. A. Knyazeva, A. A. Namgaladze, and K. E. Beloushko, Russ. J. Phys. Chem. B **9**, 758 (2015).
12. B. V. Fidel', Issled. Geomagn. Aeron. Fiz. Solntsa, No. 62, 85 (1982).
13. A. Singh and K. D. Cole, J. Atmos. Terr. Phys. **49**, 521 (1987).
14. A. D. Richmond, Pure Appl. Geophys. **131**, 413 (1989).
15. J. Du and R. J. Stening, J. Atmos. Sol.-Terr. Phys. **61**, 925 (1999).
16. V. M. Vasyliunas, in *Particles and Fields in the Magnetosphere,* Ed. by B. M. McCormac (D. Reidel, Dordrecht, 1970), p. 60.
17. M. I. Pudovkin, S. A. Zaitseva, and V. E. Zakharov, in *Polar Ionosphere and Magnetospheric-Ionospheric Relations* (IKFIA, Yakutsk, 1984), p. 3 [in Russian].
18. D. Fontaine, M. Blanc, L. Reinhart, and R. Glowinski, J. Geophys. Res. **A90**, 8343 (1985).
19. F. R. Toffoletto, S. Sazykin, R. W. Spiro, et al., J. Atmos. Sol.-Terr. Phys. **66**, 1361 (2004).
20. R. G. Roble and I. Tzur, in *Earth Electrical Environment* (Natl. Academy, Washington, DC, 1986), Chap. 15, p. 206.
21. V. V. Denisenko, Russ. J. Phys. Chem. B **9**, 789 (2015).
22. Yu. N. Korenkov, V. V. Klimenko, M. Forster, et al., J. Geophys. Res. **103**, 14697 (1998).
23. M. V. Klimenko, V. V. Klimenko, and V. V. Bryukhanov, Geomagn. Aeron. **46**, 457 (2006).
24. V. V. Klimenko, R. Yu. Luk'yanova, and M. V. Klimenko, Russ. J. Phys. Chem. B **7**, 620 (2013).
25. M. V. Klimenko, V. V. Klimenko, I. E. Zakharenkova, K. G. Ratovsky, A. S. Yasyukevich, and Yu. V. Yasyukevich, Russ. J. Phys. Chem. B **13**, 884 (2019).
26. M. V. Klimenko, V. V. Klimenko, K. G. Ratovsky, and A. S. Yasyukevich, Russ. J. Phys. Chem. B **15**, 566 (2021).
27. M. V. Klimenko, K. G. Ratovsky, V. V. Klimenko, F. S. Bessarab, T. V. Sukhodolov, and E. V. Rozanov, Russ. J. Phys. Chem. B **15**, 928 (2021).
28. M. C. Kelley, *The Earth's Ionosphere: Plasma Physics and Electrodynamics* (Academic, Burlington, 2009).
29. V. V. Klimenko, M. V. Klimenko, F. S. Bessarab, T. V. Sukhodolov, Yu. N. Koren'kov, B. Funke, and E. V. Rozanov, Russ. J. Phys. Chem. B **13**, 720 (2019).
30. V. V. Denisenko and S. S. Zamay, Planet. Space Sci. **40**, 941 (1992).
31. V. V. Denisenko, arXiv: 1802.07955 (2018).
32. V. V. Denisenko, Sib. Mat. Zh. **35**, 554 (1994).
33. V. V. Denisenko, *Energy Methods for Elliptic Equations with Nonsymmetric Coefficients* (Sib. Otdel. RAN, Novosibirsk, 1995) [in Russian].
34. V. V. Denisenko and M. J. Rycroft, J. Atmos. Sol.-Terr. Phys. **221**, 105704 (2021).
35. A. D. Richmond and A. Maute, in *Modeling the Ionosphere-Thermosphere System* (Am. Geophys. Union, Washington, DC, 2014), Chap. 6.
36. D. Bilitza, D. Altadill, V. Truhlik, et al., Space Weather **15**, 418 (2017).
37. A. D. Richmond, J. Atmos. Terr. Phys. **35**, 1083 (1973).